Journal of Power Sources 196 (2011) 8509–8518

Contents lists available at ScienceDirect

Journal of Power Sources

journal homepage: www.elsevier.com/locate/jpowsour

Thermodynamic performance analysis of a molten carbonate fuel cell at very high current densities

M.Y. Ramandi*, I. Dincer

Faculty of Engineering and Applied Science, University of Ontario Institute of Technology, Oshawa, Canada L1H 7K4

ARTICLE INFO

Article history:
Received 15 March 2011
Received in revised form 3 June 2011
Accepted 6 June 2011
Available online 16 June 2011

Keywords:
Molten carbonate fuel cell
Energy
Exergy
Efficiency
Entropy generation
Chemical exergy

ABSTRACT

This study is basically composed of two sections. In the first section, a CFD analysis is used to provide a better insight to molten carbonate fuel cell operation and performance characteristics at very high current densities. Therefore, a mathematical model is developed by employing mass and momentum conservation, electrochemical reaction mechanisms and electric charges. The model results are then compared with the available data for an MCFC unit, and a good agreement is observed. In addition, the model is applied to predict the unit cell behaviour at various operating pressures, temperatures, and cathode gas stoichiometric ratios. In the second section, a thermodynamic model is utilized to examine energy efficiency, exergy efficiency and entropy generation of the MCFC. At low current densities, no considerable difference in output voltage and power is observed; however, for greater values of current densities, the difference is not negligible. If the molten carbonate fuel cell is to operate at current densities smaller than 2500 A m^{-2}, there is no point to pressurize the system. If the fuel cell operates at pressures greater than atmospheric pressure, the unit cell cost could be minimized. In addition, various partial pressure ratios at the cathode side demonstrated nearly the same effect on the performance of the fuel cell. With a 60 K change in operating temperature, almost 10% improvement in energy and exergy efficiencies is obtained. Both efficiencies initially increase at lower current densities and then reach their maximum values and ultimately decrease with the increase of current density. By elevating the pressure, both energy and exergy efficiencies of the cell enhance. In addition, higher operating pressure and temperature decrease the unit cell entropy generation.

1. Introduction

Molten carbonate fuel cells (MCFCs) are electro-chemical energy conversion devices which exhibit low emissions, high energy conversion efficiency and flexibility regarding fuel type, representing a viable option as future low-carbon energy devices. High-temperature molten carbonate fuel cells are particularly suited for the stationary co-generation of electrical power and heat, and distributed energy supply, which enables the development and use of this technology independently from the establishment of a hydrogen infrastructure [1].

Despite the fact that MCFCs have been intensively investigated over the past few decades, the major commercialization challenges of molten carbonate fuel cells such as corrosion, short lifetime, relatively slow oxygen reduction reaction, low power density, and high cost, are still concerned [2]. In general, the goals of most ongoing investigations are to lessen the cost, extend the cell life with a stable performance and make the system more efficient.

The study of performance characteristics in MCFCs is one of the fundamental subjects of electrochemistry and has always been one of the major interests for researchers. Many studies can be found in literatures which have experimentally investigated performance of molten carbonate fuel cells (e.g. [3–6]).

In addition, some researches [7–9] are performed based on a derived 'formula for MCFC performances'. On the other hand, there are also some other studies which employ PDEs, developed by using first principles. In literatures, polarization effects, electric potentials and over-potentials are treated in various ways, mostly using experimentally derived correlations [10–12]. Previously, the volume-averaging of variables in the three phases was used as an investigational technique to develop a few polarization models [13–15]. Based on this technique, Subramanian et al. [16] developed a one dimensional, steady-state model to investigate the contribution of different cell components to losses in cell performance and showed that at low current densities, the electrolyte matrix contributes to the major fraction of potential losses. Xu et al. [17] used lattice Boltzmann method and applied Brinkman–Forchheimer-extended Darcy equations together with a

* Corresponding author. Tel.: +1 647 969 5880; fax: +1 905 721 3370.
E-mail addresses: Masoud.Youseframandi@uoit.ca (M.Y. Ramandi), Ibrahim.Dincer@uoit.ca (I. Dincer).

0378-7753/$ – see front matter © 2011 Elsevier B.V. All rights reserved.
doi:10.1016/j.jpowsour.2011.06.040

Nomenclature

a	constant coefficient of enthalpy and entropy equations
A_v	reaction surface area density ($m^2\ m^{-3}$)
A	cell active area (m^2)
C	molar concentration ($mol\ m^{-3}$)
c_p	specific heat ($J\ kg^{-1}\ K^{-1}$)
D	mass diffusivity of species ($m^2\ s^{-1}$)
F	Faraday's constant, 96,485 ($C\ mol^{-1}$)
h	enthalpy ($J\ mol^{-1}$)
i	current density ($A\ m^{-2}$)
J_0	reference exchange current density ($A\ m^{-3}$)
J	current density ($A\ m^{-2}$)
J'	volumetric current density ($A\ m^{-3}$)
K	permeability (m^2)
L	length scale (m)
$\dot{m}$	mass flux ($kg\ m^{-2}\ s^{-1}$)
M	molecular weight ($g\ mol^{-1}$)
n	number of electrons
$\dot{n}$	molar flow rate ($mol\ s^{-1}$)
P	static pressure (atm)
$\dot{Q}$	transferred heat rate (W)
R	universal gas constant 8.314 ($J\ mol^{-1}\ K^{-1}$)
s	entropy ($J\ mol^{-1}\ K^{-1}$)
S	source terms
t	time (s)
T	temperature (K)
$\vec{u}$	gas velocity ($m\ s^{-1}$)
W	width scale (m)
$\dot{W}$	Power output (W)
x	x-coordinate
X	molar fraction

Greek letters

α	transfer coefficient
β	reaction order
ε	porosity
η	over-potential (V), energy efficiency (%)
μ	dynamic viscosity ($kg\ m^{-1}\ s^{-1}$)
ν	species stoichiometric coefficient of the reaction
ϕ	electric potential (V)
Ψ	exergy efficiency (%)
Ξ	exergy ($J\ mol^{-1}$)
ρ	density ($kg\ m^{-3}$)
σ	electric conductivity ($S\ m^{-1}$)

Subscripts and superscripts

a	anode
agc	anode gas channel
c	cathode/carbonate ion
cgc	cathode gas channel
chem	chemical
d	destroyed
e	electronic
g	gas phase
gen	generation
in	inlet
i	ith component
j	jth species
m	mass equation
out	outlet
r	reversible, heat loss coefficient
s	solid
u	momentum equation
0	standard conditions
ϕ_e	electronic charge equation
ϕ_c	carbonate ion charge equation
eff	effective
ref	reference state

reaction–diffusion equation with several reasonable assumptions to generate a more realistic voltage–current density curve. Kim et al. [18] also studied the effect of water–gas shift reaction on cell performance. They figured out that even though the cell voltage and power are slightly higher when the water–gas shift reaction is included, however it is very small. In stack level models, Yoshiba et al. [19] incorporated numerical simulation to compare the stack performance of various gas-flow types. Furthermore, an interesting study was carried out by [20] to determine the behaviour of a unit MCFC at the beginning of the operation. It is worth to know that the time to achieve a steady-state was about half a second. In a study [21] for a multi-channel unit cell, it was found that the non-uniformity in fuel flow through channels deteriorates the fuel cell performance dramatically.

On the other hand, thermodynamic analysis has been used as a viable tool to investigate the energy and exergy aspects of the cogeneration systems. In fact, an MCFC permits the recovery of waste heat, which can be used in the production of steam, hot or cold water, or hot or cold air, depending on the associated recuperation equipment [22]. For instance, employing a bottoming cycle consisting of a turbine will help to supply the necessary power required for the compressors. [23]. As an effort, Silveira et al. [22], implemented the energy, exergy analysis for a cogeneration system and accomplished a global efficiency or fuel utilization efficiency of 86%. Their analysis showed that the exergy loss in the fuel cell unit is significant. Varbanov et al. [24] offered a broader view of the concept of power generation combined cycle by combining an MCFC, rather than a gas turbine, with a steam turbine. Their results showed that the inherently high power generation efficiency of the MCFC (46.38% in this case) can be significantly increased, up to nearly 70%. Kang et al. [25] simulated an externally reformed MCFC system and analyzed the effects of system configuration and operating conditions on the system efficiency for a 100 kW MCFC system. Rashidi et al. [26] performed energy and exergy analyses of a molten carbonate fuel cell hybrid system. An overall energy efficiency of 57.4%, exergy efficiency of 56.2%, bottoming cycle energy efficiency of 24.7% and stack energy efficiency of 43.4% were achieved, accordingly. Musa et al. [27] presented thermodynamic models for the internally and externally reformed MCFC and employed them in an ASPEN Customer Modeller. The results indicated that the operating temperature has more effect on the cell voltage of IR-MCFC system compared to ER-MCFC system.

Considering all previous studies, it is noticeable that the high cost of MCFCs is still an open challenge for commercialization. Operation at high current densities would be an option to lessen cell cost. Most of the previous studies have focused on the regular operating current densities (e.g. 0.1–0.25 $A\ cm^{-2}$). The scope of this research is to provide a better insight to molten carbonate fuel cell operation and performance characteristics at very high current densities (up to 0.6 $A\ cm^{-2}$) in order to reduce the molten carbonate fuel cells size, weight and consequently cost, it is essential to develop fuel cells with higher power densities. This is achieved by strictly applying balances of mass, momentum, species and charges and avoiding highly algebraic empirical correlations. Literatures usually present a polarization

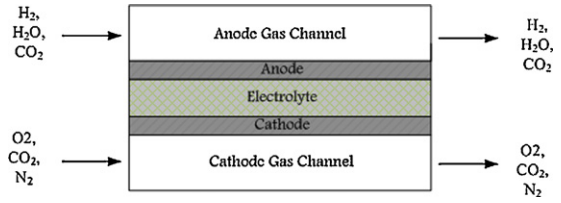

Fig. 1. The physical domain of the simulated MCFC.

curve which is derived by applying experimental correlations for electric potentials and over-potentials. However, in this study, a more complicated mathematical model, involving several coupled partial differential equations (PDEs) is used. Each phenomenon, even electric charge transfers have a separate PDE which needs to be solved using computational fluid dynamics (CFD). With the intention of prevent using highly empirical correlations for electrodes and electrolyte resistance, a diffusion model involving Butler–Volmer equation is applied to solve the electronic and ionic potential fields. From the thermodynamic point of view, literatures typically offer analysis based on the MCFC integrated systems while the exergy efficiency of the unit cell itself has been reported rarely. Hence, energy and exergy analyses are also implemented to examine efficiencies and entropy generation of the unit cell. After all, it is worthwhile to point out that in the first part of this study, a CFD analysis is carried out to obtain the characteristics of an MCFC and thermodynamic analysis is put into practice to study the entropy generation, energy and exergy efficiencies of the unit cell.

2. Problem formulation

To mathematically describe a MCFC, a comprehensive knowledge of physical and electrochemical mechanisms is required. The proposed model for the molten carbonate fuel cell, involves the conservation of mass, momentum, chemical species and electric charges.

The physical domain of the simulated MCFC is shown in Fig. 1. As it may be observed, it can be physically broken down into five individual zones: anode gas channel (AGC), anode, electrolyte, cathode and cathode gas channel (CGC). Making a theoretically rigorous fuel cell model which reflects the micro/macro-scale transport processes is extremely challenging because of a lack of experimentally evaluated physical parameters. Therefore, every numerical simulation is conceived and developed based on a set of assumptions. The following assumptions are made for the present model:

- The gas flow in the anode and cathode gas channels is laminar flow.
- The chemical species obey the ideal gas law and are ideally mixed.
- Water exists only in gaseous form.
- The porous anode and cathode are homogeneous.
- The effects of gravity are negligible.
- All reactions take place in the triple boundary phase.
- The Butler–Volmer equation is employed for the reaction in the electrodes.
- Any change in concentration of carbonate ion, CO_3^{2-}, is neglected.
- The gas mixture and solid components of fuel cell are in a thermal equilibrium state.
- The cell is operated with pure hydrogen, hence no contamination effects are considered. It is worth to mention that, in this study, fuel is considered to be supplied by an external reformer. In this reformer, natural gas which is previously mixed with steam and preheated in a regenerative heat exchanger, converts to hydrogen and carbon dioxide. The reformed gas passes through the exchanger over and over again to reduce the amount of contaminants. Next, this mixture which has a trace amount of methane and carbon monoxide is fed to the anode side of the MCFC. It is assumed that repeating the reforming process and increasing the residual time in the reformer have caused a significant reduction in the fraction of methane and carbon monoxide and hence the effect of contamination is neglected. This assumption was implemented by some other researchers who have used pure hydrogen in their simulation (e.g. [11,17,21]). However, the contaminant effects will be considered in our next study which will discuss both externally and internally reformed fuels.

Table 1
Source terms in conservation equations.

Zone	S_m	S_u	S_i	S_{ϕ_e}	S_{ϕ_c}
AGC	0	0	0	0	0
Anode	$S_{H_2}+S_{CO_2}+S_{H_2O}$	$-\frac{\varepsilon\mu}{K}u_g$	$S_{H_2}=-\frac{J'_a}{nF}$ $S_{CO_2}=\frac{J'_a}{nF}$ $S_{H_2O}=\frac{J'_a}{nF}$	J'_a	$-J'_a$
Electrolyte	0	0	0	0	0
Cathode	$S_{O_2}+S_{CO_2}$	$-\frac{\varepsilon\mu}{K}u_g$	$S_{O_2}=-\frac{1}{2}\frac{J'_c}{nF}$ $S_{CO_2}=-\frac{J'_c}{nF}$	$-J'_c$	J'_c
CGC	0	0	0	0	0

2.1. Governing equations

In general, in MCFCs fuel gas which is a gaseous mixture of hydrogen, water vapour and carbon-dioxide enters the AGC and diffuses through the porous anode where hydrogen molecules get involved into the hydrogen oxidation reaction (HOR). During this electrochemical reaction, hydrogen combines with carbonate ions, ends up to the water vapour and carbon dioxide generation. Moreover, the released electrons migrate through an external circuit, create electricity and return in to the cell through cathode. On the cathode side, a mixture of oxygen, carbon-dioxide and nitrogen enters the cathode gas channel (CGC) and diffuses through the porous cathode, where oxygen reduction reaction (ORR) takes place. Oxygen is reduced to carbonate ion by combining with carbon dioxide and the electrons coming from the external circuit. The carbonate ions formed at the cathode move through the electrolyte toward the anode, carrying the electric current and completing the carbon dioxide circuit. The underlying transport phenomena within the cell are modeled with conservation equations for mass, momentum, species and electric charges. This section exhibits the general form of these equations applied to all MCFC zones and the sink/source terms for each individual zone are summarized in Table 1.

The equation for conservation of mass, or continuity equation, can be written as follows [28]:

$$\frac{\partial}{\partial t}(\varepsilon\rho_g)+\nabla\cdot(\rho_g\vec{u}_g)=S_m \tag{1}$$

where ρ_g is the density and calculated by

$$\rho_g=\sum_{i=1}^{N}M_iC_i \tag{2}$$

In addition, S_m represents the volumetric rate of mass production/consumption which is related to the Butler–Volmer equation as described at the end of this section.

The equation for conservation of momentum is [28]:

$$\frac{\partial}{\partial t}\left(\frac{1}{\varepsilon}\rho_g\vec{u}_g\right)+\nabla\cdot\left(\frac{1}{\varepsilon^2}\rho_g\vec{u}_g\vec{u}_g\right)=-\nabla\rho_g+\nabla\cdot(\mu\nabla\vec{u}_g)+S_u \tag{3}$$

where S_u is the source/sink term of the momentum equation which is applicable just for the porous electrodes.

In fact, in this approach, the Darcy equation is utilized to model porous media. This momentum sink, contributes to the pressure gradient in the porous electrodes, creating a pressure drop that is proportional to the fluid velocity. For a homogeneous porous media;

$$S_u = -\frac{\varepsilon\mu}{K}u_g \tag{4}$$

where K is the permeability of the porous media and is determined by

$$K = \frac{D_P^2}{150}\frac{\varepsilon^3}{(1-\varepsilon)^3} \tag{5}$$

To describe the chemical species transport, Eq. (6) is considered which is the general form of the conservation equation including both convection and diffusion terms [28].

$$\frac{\partial}{\partial t}(\varepsilon C_i) + \nabla\cdot(-D_{i,m}^{eff}\nabla C_i) + \nabla\cdot(\vec{u}_g C_i) = S_i \tag{6}$$

The effective mass diffusion coefficient for species i in the mixture, $D_{i,m}^{eff}$, is calculated by

$$D_{i,m}^{eff} = \frac{1-X_i}{\sum_{j,j\neq i}^{N}(X_j/D_{ij}^{eff})} \tag{7}$$

where D_{ij}^{eff} is the effective binary mass diffusion coefficient of component i in component j and is calculated using

$$D_{ij}^{eff} = D_{ij}\frac{T}{T_{ref}}\cdot\frac{P_{ref}}{P}\cdot\varepsilon^{1.5} \tag{8}$$

Before moving on to the electric transport equations, it is worth to mention that in a porous electrode the local electrochemical reaction rate depends on the driving force, the local over-potential, i.e., the divergence from the equilibrium potential. Therefore, it is preferable to use the potential instead of the current in the transport equation [29]. Furthermore, the current density is a vector quantity, and only the transverse component (normal to the electrode surface) is functional and contributes to the power output of the cell; the lateral component only decreases the cell output [30].

The charge conservation equations describe the electric current in electrically conductive components and ionic current in ionic conductive components. Any change in concentration of carbonate ion, CO_3^{2-}, is neglected which consequently means that the effect of migration can be neglected as well. Therefore, Ohms' law is valid in MCFC zones for both electronic charge and ionic charge. Hence, the conservation of electronic charge can be written as

$$0 = \nabla\cdot(-\varepsilon^{1.5}\sigma_e\nabla\phi_e) - S_{\phi_e} \tag{9}$$

and the conservation equations of ionic charge is

$$0 = \nabla\cdot(-\varepsilon^{1.5}\sigma_c\nabla\phi_c) - S_{\phi_c} \tag{10}$$

It should be pointed out that, with the intention of simplifying, the unit cell is considered to operate in isothermal condition. It is worthwhile to mention that each transport phenomena is represented by a general form of conservation equation which takes the porosity into consideration. Clearly, the porosity ranges from zero to one for various zones. Finally, the Buttler–Volmer equation which describes the net withdrawn current density in fuel cells is used to determine various source terms of the MCFC.

$$J_a' = A_{v,a}J_{o,a}^{ref}\left(\frac{C_{R,a}}{C_{R,a}^{ref}}\right)^{\beta_a}\left[\exp\left(\frac{\alpha_{a,a}nF\eta_a}{RT}\right) - \exp\left(-\frac{\alpha_{c,a}nF\eta_a}{RT}\right)\right] \tag{13}$$

$$J_c' = A_{v,c}J_{o,c}^{ref}\left(\frac{C_{R,c}}{C_{R,c}^{ref}}\right)^{\beta_c}\left[\exp\left(\frac{\alpha_{a,c}nF\eta_c}{RT}\right) - \exp\left(-\frac{\alpha_{c,c}nF\eta_c}{RT}\right)\right] \tag{14}$$

2.2. Boundary conditions

With the purpose of completing the MCFC model formulation, specifying various boundary conditions at different positions are critical. The boundary conditions, for a computational domain with a single pair of gas flow channels, are illustrated in Fig. 2. At the anode gas channel inlet (I_{agc}) and cathode gas channel inlet (I_{cgc}), the total mass flux and gas species composition of the entering gas flow are specified. Moreover, the fluxes of electric and ionic charge are considered to be zero. Additionally, considering the very large aspect ratio (length to height ratio) of the gas channels, the flow is assumed to be fully developed at the anode gas channel outlet (O_{agc}) and cathode gas channel outlet (O_{cgc}). This means, none of the variable fluxes vary in the normal direction. Likewise, the gas pressure is specified. A no slip boundary condition is applied to the anode and cathode gas channel walls including, W_{agc}^T, W_{cgc}^B.

The fluxes of electric and ionic charge are set to zero. For all other walls of the gas channels, $W_{a,agc}^L$, $W_{a,agc}^R$, $W_{c,cgc}^L$, and $W_{c,cgc}^R$, the electronic potential is specified while, the flux of the remaining variables is set as zero. For the no-flux boundaries, Z^L and Z^R, the zero flux condition is assumed for all variables.

3. Numerical study

The Finite Volume Method is employed to simulate the operation of the molten carbonate fuel cells. The computational domain is defined and divided into a number of control volumes using ANSYS ICEM CFD 12.0.1. To handle the divergence difficulties, a set of under-relaxation techniques is developed. The governing equations are discretized using commercial software, ANSYS FLUENT 12.0.1. The C programming language is used to develop a code in order to add several capabilities to ANSYS FLUENT 12.0.1. The SIMPLE algorithm is selected for the coupling between the pressure and velocity field. An algebraic multi-grid (AMG) method with a Gauss–Seidel type smoother is used to accelerate the convergence. A strict convergence criterion with a residual of 10^{-8} is used for all variables.

4. Thermodynamic analysis

Thermodynamics plays a critical role in the analysis of processes, systems and devices in which energy transfers and energy transformations take place [31]. In this regard, energy analysis is the traditional method of assessing the way energy is used. However, an energy balance provides no information on the degradation of energy or resources and does not quantify the usefulness or quality of the various energy and material streams flowing through a system and exiting as products and wastes [31]. On the other hand, exergy analysis is a useful tool for furthering the goal of more efficient energy use, as it enables the determination of the location, type and true magnitude of energy wastes and losses in a system [32]. Exergy is defined as the maximum amount of work which can be obtained from a system or a flow of matter when it is brought reversibly to equilibrium with the reference environment. Exergy analysis is based on second law of thermodynamics and the concept of irreversible entropy production. The exergy consumption during a process is proportional to the entropy production due to irreversibilities.

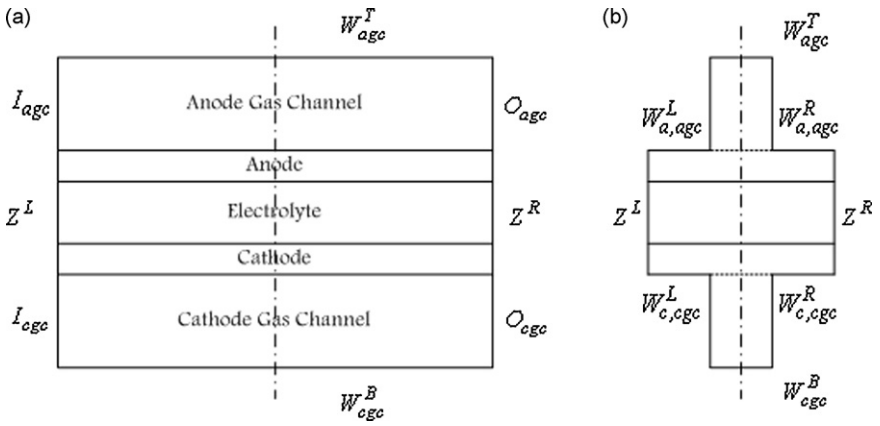

Fig. 2. Boundary conditions for the MCFC model: (a) front view, (b) side view.

In order to investigate the performance of the MCFC in thermodynamics point of view, the molten carbonate fuel cell is treated as a black box with two inputs and two output streams (Fig. 3) and the energy and exergy balances are applied for the unit cell. In this fashion, energy and exergy efficiencies of the unit cell are defined accordingly.

It is worthwhile to mention that this research is to present performance characteristics of a 'unit cell'. Generally, the inlet streams are taken from external devices as they are. Therefore, no calculation is performed out of the unit cell boundaries, as estimating the parasitic losses is not in the scope of this study.

First of all, for a specified operating current density, components molar usage and production can be calculated. Therefore, a molar balance results

$$\dot{n}_{H_2}^{a,in} = \dot{n}_{H_2}^{a,out} + \frac{i_{MCFC}A_{MCFC}}{nF} \tag{15}$$

$$\dot{n}_{H_2O}^{a,in} + \frac{i_{MCFC}A_{MCFC}}{nF} = \dot{n}_{H_2O}^{a,out} \tag{16}$$

$$\dot{n}_{CO_2}^{a,in} + \frac{i_{MCFC}A_{MCFC}}{nF} = \dot{n}_{CO_2}^{a,out} \tag{17}$$

$$\dot{n}_{O_2}^{c,in} = \dot{n}_{O_2}^{c,out} + \frac{i_{MCFC}A_{MCFC}}{2nF} \tag{18}$$

$$\dot{n}_{CO_2}^{c,in} = \dot{n}_{CO_2}^{c,out} + \frac{i_{MCFC}A_{MCFC}}{nF} \tag{19}$$

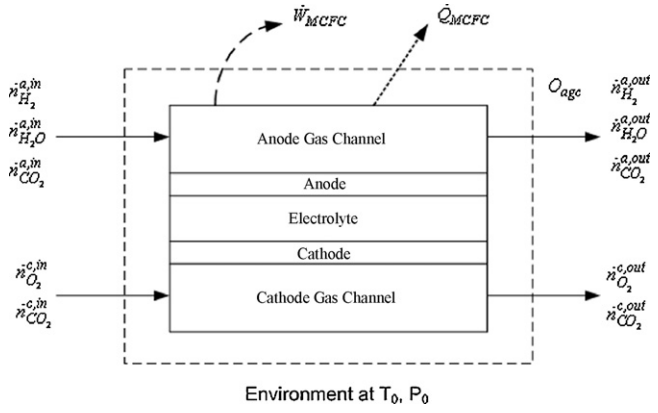

Fig. 3. Schematic of the fuel cell and system boundaries studied in energy and exergy analyses.

The energy balance of the unit cell can be written as follows:

$$\sum_{i=1}^{N}\dot{n}_i^{a,in}h_i^{a,in} + \sum_{i=1}^{N}\dot{n}_i^{c,in}h_i^{c,in} = \sum_{i=1}^{N}\dot{n}_i^{a,out}h_i^{a,out} + \sum_{i=1}^{N}\dot{n}_i^{c,out}h_i^{c,out} + \dot{Q}_{MCFC} + \dot{W}_{MCFC} \tag{20}$$

Accordingly, the exergy balance reads

$$\sum_{i=1}^{N}\dot{n}_i^{a,in}\Xi_i^{a,in} + \sum_{i=1}^{N}\dot{n}_i^{c,in}\Xi_i^{c,in} = \sum_{i=1}^{N}\dot{n}_i^{a,out}\Xi_i^{a,out} + \sum_{i=1}^{N}\dot{n}_i^{c,out}\Xi_i^{c,out} + \left(1-\frac{T_0}{T}\right)r\dot{Q}_{MCFC} + \dot{W}_{MCFC} + \Xi_d \tag{21}$$

where $\dot{Q}_{MCFC}$, $\dot{W}_{MCFC}$ and Ξ_d denote the heat transferred by MCFC walls, the output electrical power of the MCFC and the destroyed exergy ($T.\dot{s}_{gen}$), respectively.

The molar exergy term is evaluated by a summation over physical, thermal and chemical exergetic terms. Therefore

$$\Xi_i = ([h_i(T) - h_i(T_0)] - T_0[s_i(T) - s_i(T_0)]) + RT_0\ \ln(X_i) + \Xi_i^{chem} \tag{22}$$

where X_i is the molar fraction of component i and Ξ_i^{chem} is the chemical exergy which are found from [33].

With the purpose of evaluating molar enthalpy and entropy of each species, and assuming that the gases in anode gas channel and cathode gas channel obey the ideal gas behaviour, the following polynomial equations fitted to the data, taken from JANAF table used in [34].

$$\frac{h}{RT} = \left(a_1 + \frac{a_2}{2}T + \frac{a_3}{3}T^2 + \frac{a_4}{4}T^3 + \frac{a_5}{5}T^4 + \frac{a_6}{T}\right) \tag{23}$$

$$\frac{s}{RT} = \left(a_1\ \ln(T) + a_2T + \frac{a_3}{2}T^2 + \frac{a_4}{3}T^3 + \frac{a_5}{4}T^4 + a_7\right) \tag{24}$$

Furthermore, the output power of the unit cell is calculated as follows:

$$\dot{W}_{MCFC} = i_{MCFC}\cdot A_{MCFC}\cdot V_{MCFC} \tag{25}$$

where A_{MCFC} is the active surface area of MCFC and i_{MCFC} is the operating current density. The cell voltage is determined by

$$V_{MCFC} = E_r - i_{MCFC}(\eta_{act} + \eta_{conc} + \eta_{ohm}) \tag{26}$$

where E_r is the reversible open circuit voltage. Likewise, η_{act}, η_{conc} and η_{ohm} are the activation, concentration and ohmic impedances,

Table 2
The structural parameters of the simulated MCFC.

Parameter	Value
Anode gas channel height (mm)	0.2
Anode height (mm)	0.07
Electrolyte height (mm)	1.0
Cathode height (mm)	0.06
Cathode gas channel height (mm)	0.2
Cell length (mm)	100
Cell width (mm)	100
Porosity of anode, ε_a	0.52
Porosity of cathode, ε_c	0.62

respectively. These parameters are estimated by the available empirical correlations in the literature [35].

$$E_r = E_0 + \left[\frac{RT}{2F}\ln\left(\frac{P_{H_2,a}P_{CO_2,c}P_{O_2,c}^{0.5}}{P_{CO_2,a}P_{H_2O,a}}\right)\right] \quad (27)$$

$$E_0 = 1.2723 - 2.7645\times10^{-4}T \quad (28)$$

$$\eta_{act} = 2.27\times10^{-9}\times\exp\left(\frac{6435}{T}\right)\times P_{H_2}^{-0.42}\times P_{CO_2}^{-0.17}\times P_{H_2O}^{-1.0} \quad (29)$$

$$\eta_{conc} = 7.505\times10^{-10}\times\exp\left(\frac{9298}{T}\right)\times P_{O_2}^{-0.43}\times P_{CO_2}^{-0.09} \quad (30)$$

$$\eta_{ohm} = 0.5\times10^{-4}\times\exp\left[3016\times\left(\frac{1}{T}-\frac{1}{923}\right)\right] \quad (31)$$

In addition, the heat transferred by MCFC walls is

$$\dot{Q}_{MCFC} = T(\Delta s - s_{gen}) \quad (32)$$

where s_{gen} is calculated by

$$s_{gen} = \frac{2F}{T}(\eta_{act}+\eta_{conc}+\eta_{ohm}) \quad (33)$$

Finally, the energy and exergy efficiencies of the molten carbonate fuel cell are evaluated by

$$\eta = \frac{\dot{W}_{MCFC}}{\sum_{i=1}^{N}\dot{n}_i^{a,in}h_i^{a,in}+\sum_{i=1}^{N}\dot{n}_i^{c,in}h_i^{c,in}} \quad (34)$$

$$\psi = \frac{\dot{W}_{MCFC}}{\sum_{i=1}^{N}\dot{n}_i^{a,in}\Xi_i^{a,in}+\sum_{i=1}^{N}\dot{n}_i^{c,in}\Xi_i^{c,in}} \quad (35)$$

5. Results and discussion

5.1. CFD results

The system of conservation equations were solved after fixing some field variables for various operating conditions using the specifications described in Table 2. In order to investigate the effects of temperature, pressure, current density and cathodic partial pressure ratio, the voltage–current density, power–current density and overpotential–temperature curves were plotted at different conditions. In a simple case, model prediction for voltage–current density curve was compared with the literature data [17]. Fig. 4 shows the validated results. As may be observed from this figure, a good agreement was obtained.

Next, for each of the cases that are studied in this research, the unit cell was assumed to be isothermal and operate at a temperature of 883, 903 and 923 K. The operating pressure of the cell was set to be 1, 2 and 3 atm and the cathodic stoichiometric ratios of 0.5, 1.0 and 2.0 were selected.

Figs. 5 and 6 demonstrate the effects of temperature on polarization curves and power–current density curves, respectively, for three different operating temperatures (883, 903 and 923 K). For this case, the operating pressure was assumed to be atmospheric.

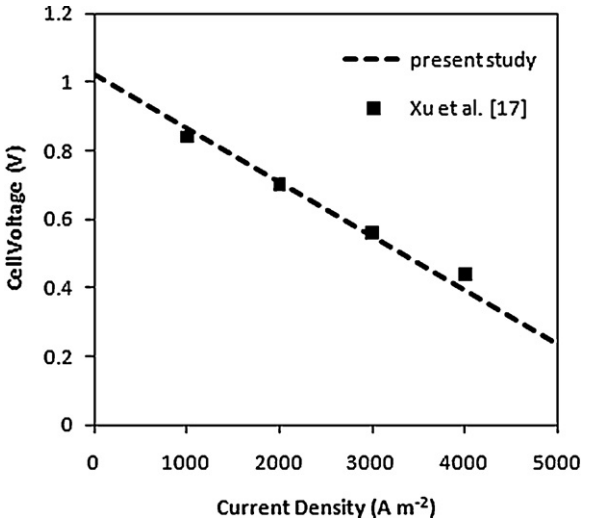

Fig. 4. Comparison of model prediction with the literature data [17].

The fuel gas component mole fractions for H_2, H_2O and CO_2 were 0.7, 0.2 and 0.1, respectively. Furthermore oxidant was assumed to be consisting of O_2, CO_2 and N_2 with the mole fractions of 0.15, 0.30 and 0.55, correspondingly. From the results shown in Fig. 5, it may be observed that for low current densities (up to 2000 A m^{-2}), there is not a significant difference in cell output voltage and power, but for higher values of current densities, the difference is not negligible. More specifically, a 20 K temperature reduction lowers the output power almost 20%. In addition, it is clear that an increase in operating temperature results a higher output voltage. As it is mentioned earlier, fuel cells with high current densities are demanded to reduce the cost. But Fig. 5 shows that the cell output voltage decreases as the current density increases. Therefore, an investigation is required to figure out what the optimum operating current density is. This could be achieved by plotting power versus current density at different operating temperatures as shown in Fig. 6. According to this figure, the output power grows with an increase in current density up to the point where the overall trend begins to be diminished. This is the point in which power has its highest value and current density also is relatively high. This pair of current density and power could be used for unit cell design considera-

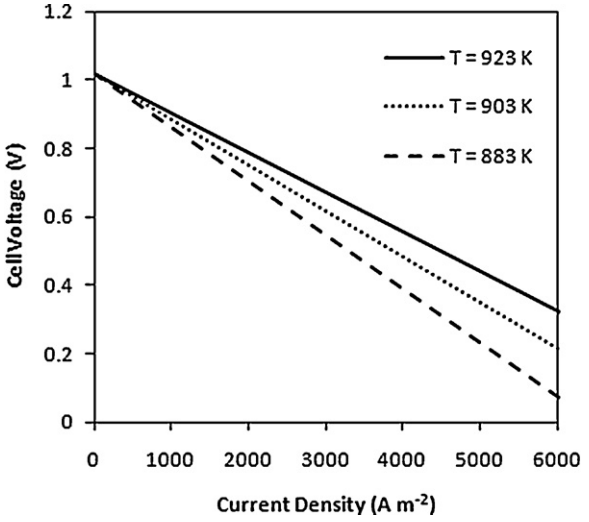

Fig. 5. Effect of temperature on polarization curve (operating condition: atmospheric pressure, fuel gas: 0.7 H_2/0.2 H_2O/0.1 CO_2 and 0.15 O_2/0.3 CO_2/0.5 N_2 as oxidant).

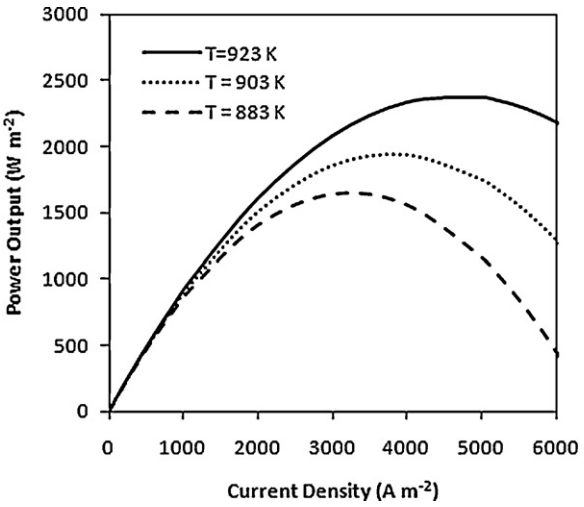

Fig. 6. Effect of temperature on output power (operating condition: atmospheric pressure, fuel gas: 0.7 H_2/0.2 H_2O/0.1 CO_2 and 0.15 O_2/0.3 CO_2/0.5 N_2 as oxidant).

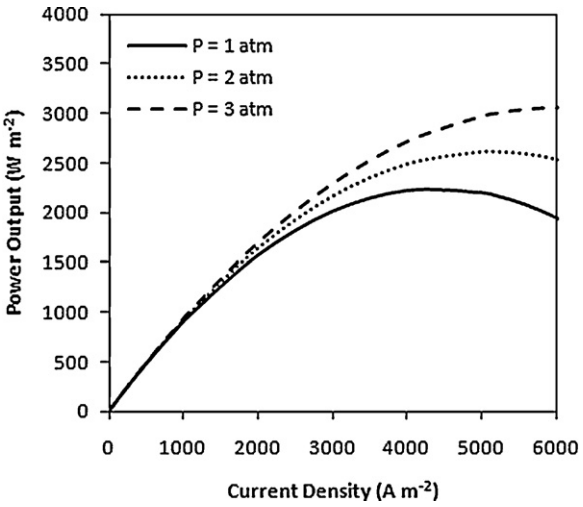

Fig. 8. Effect of pressure and current density on cell power (operating condition: 923 K, fuel gas: 0.7 H_2/0.2 H_2O/0.1 CO_2 and 0.15 O_2/0.3 CO_2/0.5 N_2 as oxidant).

tions. For an operating temperature of 883 K, the maximum power occurs at the current density of 3000 A m^{-2} while a 40 K temperature increase enables the system to enhance its maximum power by 1000 A m^{-2}. In fact, by raising the unit cell operating temperature, the maximum power shifts to the right side of the horizontal axis, which consequently results in a higher current density.

The variations in voltage losses with changes in temperature are presented in Fig. 7. For this case, three different current densities (1500, 2000 and 2500 A m^{-2}) were chosen. The fuel gas and oxidant composition and cell operating pressure were assumed to be the same as the previous case. This figure illustrates the reason behind the decreasing tendency in cell output voltage as the current density becomes more intense. These losses are caused by the polarization effects. The study of polarization losses is one of the main subjects of electrochemistry application in fuel cells. The irreversibilities occurring in a fuel cell electrochemical reaction degrade the unit cell output voltage in form of over-potentials. According to Fig. 7, the fuel cell voltage losses drop as the temperature increases in an almost linear fashion for all operating current densities. In addition, at any temperature, higher polarizations are caused by greater operating current densities. In fact, as current density increases, the electrochemical reaction rates become enhanced which, consequently, heightens the consumption/production rate of chemical gaseous species, surges the system irreversibilities and hence creates voltage losses when the drawn current density is increased.

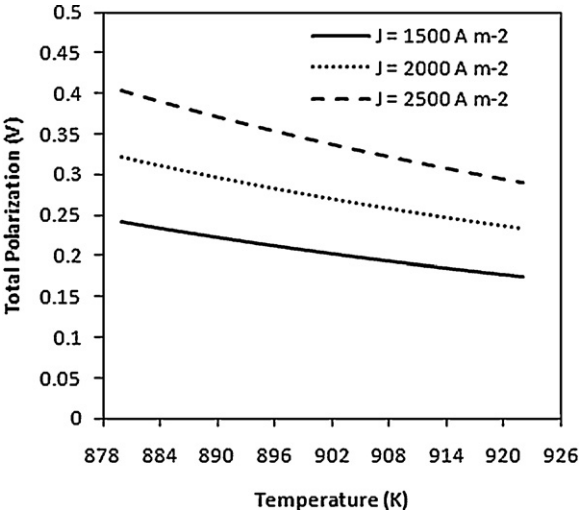

Fig. 7. Effect of temperature and current density on total polarization (operating condition: atmospheric pressure, fuel gas: 0.7 H_2/0.2 H_2O/0.1 CO_2 and 0.15 O_2/0.3 CO_2/0.5 N_2 as oxidant).

Fig. 8 presents the output power versus current density for various operating pressure (1 atm, 2 atm and 3 atm). Fuel gas and oxidant compositions were set to be the same as the previous case studies and the operating temperature was fixed at 923 K. As shown in this figure, it is obvious that for low current densities (up to 2500 A m^{-2}), there is not a significant difference in output power. Therefore, if the molten carbonate fuel cell is to operate at current densities smaller than 2500 A m^{-2}, there is no point to pressurize the system and accordingly augment the cost. However, it may be observed from this figure that for any current density, the output power is enhanced as the operating pressure is increased. In addition, the maximum power occurs at higher current densities for greater pressures. It may be perceived that if the fuel cell operates at pressures greater than atmospheric pressure, the system will be capable of generating greater values of power which, economically, could lessen the costs. However, it should be pointed out that pressurizing the unit cell results in higher partial pressure of the fuel and oxidant components which contribute in the electrochemical reactions and subsequently, decrease the irreversibilities leading to a higher output voltage.

In practice, the benefits of pressurized operation are momentous just up to about 3–4 bar. However, existing manufacturers do not operate their MCFC systems at very higher pressures. Without a doubt there are disadvantages associated with the higher operating pressures brought by the system design constraints. In general, it is thought that pressurizing the MCFC systems is not economical for the output power less than 1 MW. There are important power costs involved in compressing the reactant gases. The costs involved with operating at high pressure are those connected with the extra mass involved with designing a high-pressure system. Contrasting the benefits of increased pressure are the effects on unwanted side reactions such as carbon deposition (Boudouard reaction). The problem of leaks from high-pressure systems is obviously another crucial concern. The MCFC system needs to be designed with the least possible chance of any leaks and should be monitored for such leaks on a regular basis. Apart from the waste of gas, there is also the likelihood of the build-up of explosive mixtures of hydrogen and oxygen. To sum up, it is crucial to select the operating pressure, accurately.

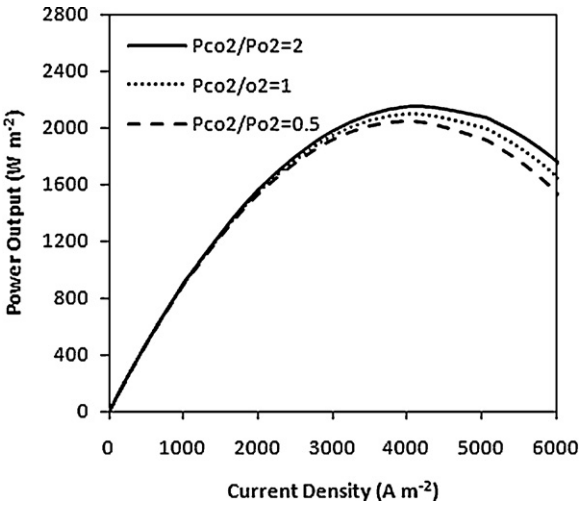

Fig. 9. Effect of current density and P_{CO_2}/P_{O_2} ratio on cell power (operating condition: 923 K, fuel gas: 0.7 H_2/0.2 H_2O/0.1 CO_2).

Fig. 9 illustrates the power–current density curve of the cell for different ratios of carbon-dioxide and oxygen (2.0, 1.0 and 0.5) fed into fuel cell. The operating temperature and pressure were assumed to be 923 K and atmospheric, respectively. It appears that the variation of this ratio has no significant effect on the cell output power. However, the figure demonstrates a slight difference at higher ratios which indicates that the excess carbon dioxide is desired. The same conditions and arguments are applicable in describing the voltage–current density curve (Fig. 10). The linear behaviour of the polarization curve for molten carbonate fuel cells, as is proved in this study, is normal. The reason is that the activation polarization which happens at low current densities in the low-temperature fuel cell (e.g. proton exchange membrane fuel cell), disappears in a high-temperature fuel cells. This observable fact was also reported in some other studies [13,17].

In conclusion, in view of the fact that the current density is a vector quantity, it is worth to mention that only the transverse component is valuable and contributes to the output power of the cell. In other words, the lateral component only diminishes the output power. Precisely, for the electrochemical reaction occurring in the triple boundary phase, electrons must transfer transversely through the electrode to be collected. Thus, in every stage of molten carbonate fuel cell design, endeavour must be implemented to minimize the lateral component.

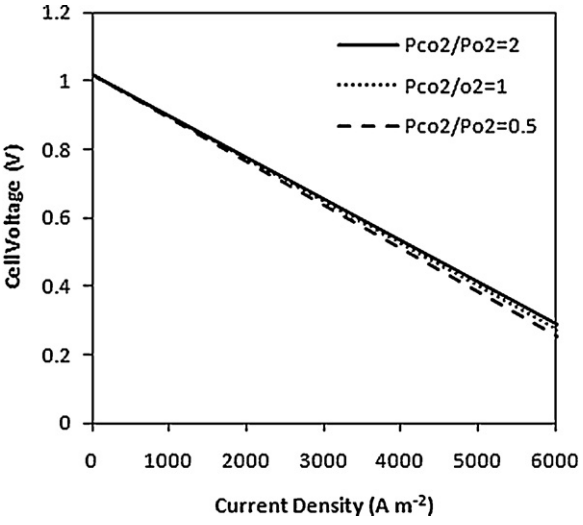

Fig. 10. Effect of current density and P_{CO_2}/P_{O_2} ratio on cell voltage (operating condition: 923 K, fuel gas: 0.7 H_2/0.2 H_2O/0.1 CO_2).

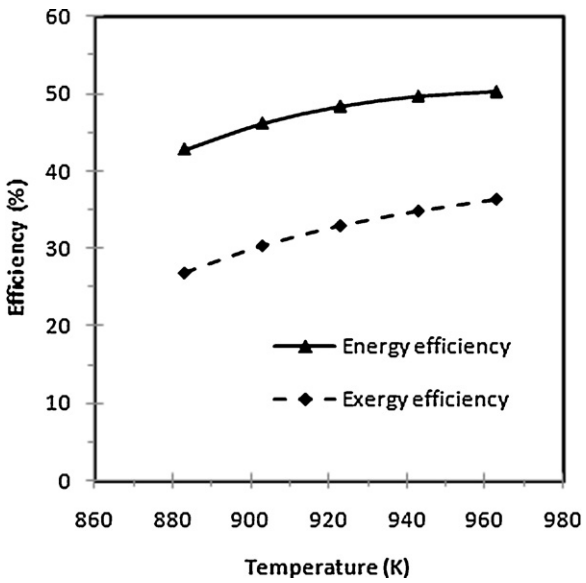

Fig. 11. Variations of cell energy and exergy efficiencies at different operating temperatures.

5.2. Thermodynamic results

In this section, a number of parametric studies were conducted in details with the intention of estimating the performance of the molten carbonate fuel cell with different operating conditions. Using equations provided earlier, energy and exergy efficiencies of the unit cell were obtained. In addition, the entropy generation is investigated in some cases. In general, molar fractions of hydrogen, water vapour and carbon dioxide were considered to be 0.72, 018 and 0.1, respectively. Likewise, oxygen and carbon dioxide molar fractions were chosen to be 0.33 and 0.67. Anodic and cathodic gas flow rates are 1.66 mol h^{-1} and 2.04 mol h^{-1}, respectively, unless otherwise stated.

Variations of cell energy and exergy efficiencies at different operating temperatures (ranging from 883 K to 963 K) are presented in Fig. 11. Results were obtained based on operating current density of 4000 A m^{-2} and atmospheric pressure. According to Fig. 11, energy efficiency of the unit cell varies from 42.8% to 50.5% while the exergy efficiency remains in the range of 26.8–36.3%. The dissimilarity of the two aforementioned efficiencies is caused by internal irreversibilities. Perceptibly, the activation, ohmic and concentration polarizations are the major source of irreversibilities and hence, exergy destroyed inside the fuel cell assembly. As a result, the destroyed exergy diminishes the exergy efficiency of the MCFC. However, it is apparent that both energy and exergy efficiencies enhance with the increase of temperature. This effect can be justified with the fact that an increase in operating temperature reduces the irreversible losses (irreversibility) of the fuel cell, which in turn results in augment of both energy and exergy efficiencies. Furthermore, as it may be observed from Fig. 11, even though both efficiencies increase with temperature, a sharper trend takes place in lower temperatures and they tend to have a flatter shape at higher temperatures. In fact, the unit cell total losses and the total input energy and exergy are the origin of this alteration in the efficiency trends. Clearly, Eqs. (29)–(31) illustrate that as temperature increases, the activation, ohmic and concentration losses (hence total polarization) drop. The higher the temperature reaches, the lower the irreversibilities are. In contrast, escalating the tempera-

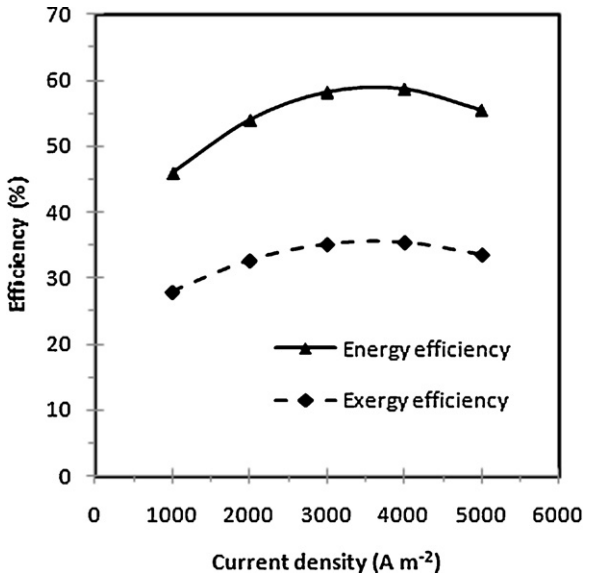

Fig. 12. Variations of cell energy and exergy efficiencies at different current densities.

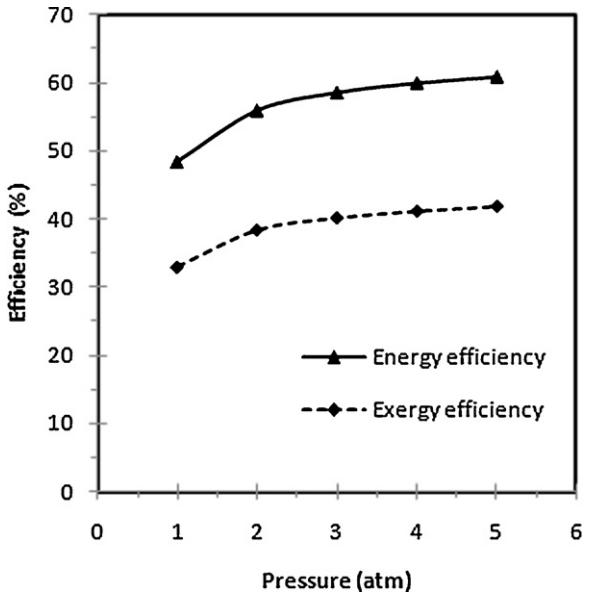

Fig. 13. Variations of cell energy and exergy efficiencies at different operating pressures.

ture results in a constant increase of energy and exergy supplied to the unit cell while the net power output of the cell reaches a maximum and then declines. As a consequence, efficiencies are expected to decrease. There always seems to be a trade off between the effect of ohmic losses and supplied energy and exergy.

Fig. 12, presents the effect of current density (ranging from 1000 to 5000 A m^{-2}) on energy and exergy efficiencies. For this case, the operating temperature and pressure were set to 883 K and 2 atm, respectively. It may be observed that both energy and exergy efficiencies initially raise at lower current densities up to the point that they attain their maximum values and ultimately decrease with the increase of current density. In terms of energy and exergy efficiencies, the optimum current density occurs around 4000 A m^{-2}. At the optimum current density, 58.7% energy efficiency and 35.5% exergy efficiency were achieved. Since the operating temperature is considered to be constant, any change in both efficiencies can be attributed to the net power output of the MCFC which is a function of cell operating voltage and current density. As it is already discussed in Section 5.1, the voltage–current density curve has an increasing–decreasing trend which concludes a similar fashion in both efficiencies.

Effects of operating pressure (1–5 atm) on energy and exergy efficiencies of the studied MCFC are illustrated in Fig. 13. In this parametric study, the operating temperature and current density were considered to be 923 K and 4000 A m^{-2}. With the increase of pressure, both the energy and exergy efficiencies of the cell enhance. This is realistic since as pressure increases, an extensive drop in irreversible losses occurs. In particular, anode and cathode over-potentials get lower values in higher pressures. To be more specific, molar concentration of hydrogen in anodic triple phase boundary, and oxygen and carbon dioxide in cathodic triple phase boundary increase with an increase in operating pressure. As a consequence, the irreversible losses of anode and cathode decrease, which in turn improve the performance of the MCFC. Nevertheless, both efficiencies' increase is sharper at the operating pressures below 3 atm and they tend to have a smoother change above this pressure.

Fig. 14 describes how the variation of anode/cathode gas flow ratio can affect the efficiencies of an MCFC. The unit cell assumed to operate at 923 K, atmospheric pressure and 4000 A m^{-2}. Results show that an increase in this stoichiometric ratio lessens the energy and exergy efficiencies of the unit cell. These changes are considerable for energy efficiency rather than exergy efficiency. Moreover, it may be observed from Fig. 14 that, as this ratio grows over the unity, both efficiencies decrease with a gentle slope. In addition, both efficiencies have their peak value when the molar flow rate of the oxidant entering cathode gas channel is higher than the fuel molar flow rate which gets into the anode gas channel.

Table 3
Variations of entropy generation at different operating temperatures and pressures.

Temperature (K)	Entropy generation (J mol^{-1} K^{-1})	Pressure (atm)	Entropy generation (J mol^{-1} K^{-1})
883	26.2	1	19.7
903	22.6	2	15.8
923	19.7	3	13.6
943	17.4	4	12.9
963	15.4	5	12.4

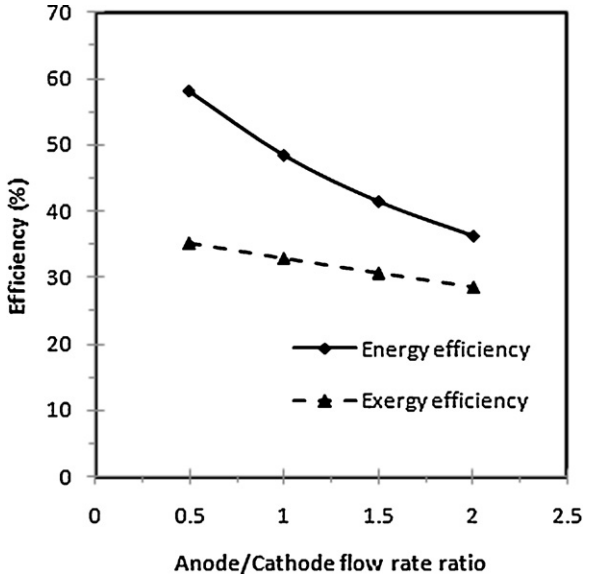

Fig. 14. Variations of cell energy and exergy efficiencies at different anode/cathode flow rate ratios.

Table 3 summarizes the value of the unit cell entropy generation at different operating temperatures and pressures. As it may be seen from this table, an increase in operating temperature decreases the entropy generation in the unit cell. This effect can be acceptable by noting the fact that, the entropy generation is a function of cell irreversibilities in terms of activation and ohmic polarization. These irreversibilities, as shown in Fig. 7, are considerably reduced with the increase of operating temperature, which in turn cause a drop in the entropy generation. Likewise, higher operating pressures result in lower irreversibilities and hence entropy generation.

6. Conclusions

In the first part of this study, a mathematical model is developed to investigate the performance characteristics of a molten carbonate fuel cell at very high current densities, by employing mass and momentum conservation, electrochemical reaction mechanisms and electric charge transfer. A finite volume based commercial software package, ANSYS FLUENT 12.0.1, is used to solve the system of PDE equations. In addition, the model was applied to predict the unit cell performance characteristics at a variety of operating pressures, temperatures, and cathode gas stoichiometric ratios. The present results confirm the following:

- For low current densities, there is not very significant difference in output voltage and power. However for greater values of current densities, the difference is not negligible.
- The fuel cell total voltage loss drops as the temperature increases in an almost linear fashion for all operating current densities.
- If the molten carbonate fuel cell is to operate at current densities smaller than 2500 A m^{-2}, there is no point to pressurize the system.
- Above this current density, the output power is enhanced as the operating pressure is increased, nevertheless.
- If the fuel cell operates at pressures greater than atmospheric pressure, the unit cell cost could be minimized.
- Various partial pressure ratios at the cathode side, demonstrated nearly the same effect on the performance of the fuel cell.

In the second part, a thermodynamic model is utilized to examine energy efficiency, exergy efficiency and entropy generation of the MCFC. Some parametric studies are performed and the following results are obtained:

- By changing the operating temperature from 883 K to 963 K, the energy efficiency of the unit cell varies from 42.8% to 50.5% while the exergy efficiency remains in the range of 26.8–36.3%.
- Both efficiencies initially raise at lower current densities up to the point that they attain their maximum values and ultimately decrease with the increase of current density.
- With the increase of pressure, both the energy and exergy efficiencies of the cell enhance.
- An increase in this anode/cathode flow ratio lessens the energy and exergy efficiencies of the unit cell.
- Higher operating pressure and temperature decrease the unit cell entropy generation.

Acknowledgements

The support for this research by the Ontario Research Fund and the Natural Sciences and Engineering Research Council of Canada is gratefully acknowledged.

References

[1] P.P. Edwards, V.L. Kuznetsov, W.I.F. David, N.P. Brandon, Energy Policy 36 (2008) 4356–4362.
[2] G. De Simon, F. Parodi, M. Fermegila, R. Taaccani, Journal of Power Sources 115 (2003) 210–218.
[3] E. Fontes, C. Lagergren, D. Simonsson, Journal of Electroanalytical Chemistry 432 (1997) 121–128.
[4] J. Brouwer, F. Jabbari, E.M. Leal, T. Orr, Journal of Power Sources 158 (2006) 213–224.
[5] C.G. Lee, B.S. Kang, H.K. Seo, H.C. Lim, Journal of Electroanalytical Chemistry 540 (2003) 169–188.
[6] E. Arato, B. Bosio, R. Massa, F. Parodi, Journal of Power Sources 86 (2000) 302–308.
[7] Y. Mugikura, T. Abe, T. Watanabe, Y. Izaki, Denki Kagaku 60 (1992) 124–130.
[8] H. Morita, Y. Mugikura, Y. Izaki, T. Watanabe, T. Abe, Denki Kagaku 63 (1995) 1053–1060.
[9] F. Yoshiba, T. Abe, T. Watanabe, Journal of Power Sources 87 (2000) 21–27.
[10] M. Baranak, H. Atakul, Journal of Power Sources 172 (2007) 831–839.
[11] H. Hao, H. Zhang, S. Weng, M. Su, Journal of Power Sources 161 (2006) 849–855.
[12] M.J. Yoo, D.P. Kim, G.Y. Chung, H.C. Lim, Journal of Fuel Cell Science and Technology 3 (2006) 327–332.
[13] N. Subramanian, B.S. Haran, P. Ganesan, R.E. White, B.N. Popov, Journal of the Electrochemical Society 150 (2003) A46–A56.
[14] J.A. Prins-Jansen, K. Hemmes, H.W. De Wit, Electrochimica Acta 42 (1997) 3585–3600.
[15] P. De Vidts, R.E. White, Journal of the Electrochemical Society 144 (1997) 1343–1353.
[16] N. Subramanian, B.S. Haran, R.E. White, B.N. Popov, Journal of the Electrochemical Society 150 (2003) A1360–A1367.
[17] Y.S. Xu, Y. Liu, X.Z. Xu, G.X. Huang, Journal of the Electrochemical Society 153 (2006) A607–A613.
[18] M.H. Kim, H.K. Park, G.Y. Chung, H.C. Lim, S.W. Nam, T.H. Lim, A.A. Hong, Journal of Power Sources 104 (2002) 245–252.
[19] F. Yoshiba, N. Ono, Y. Izaki, T. Watanabe, T. Abe, Journal of Power Sources 71 (1998) 328–336.
[20] Y.R. Lee, I.G. Kim, G.Y. Chung, C.G. Lee, H.C. Lim, T.H. Lim, S.W. Nam, S.A. Hong, Journal of Power Sources 137 (2004) 9–16.
[21] Z. Ma, S.M. Jeter, A.I. Abdel-Khalik, International Journal of Hydrogen Energy 28 (2003) 85–97.
[22] J.L. Silveira, E.M. Leal, L.F. Ragonha Jr., Energy 26 (2001) 891–904.
[23] R. Rashidi, P. Berg, I. Dincer, International Journal of Hydrogen Energy 34 (2009) 4395–4405.
[24] P. Varbanov, J. Klemes, R.K. Shah, S. Harmanjeet, Journal of Fuel Cell Science and Technology 3 (2006) 375–383.
[25] B.S. Kang, J.H. Koh, H.C. Lim, Journal of Power Sources 108 (2002) 232–238.
[26] R. Rashidi, I. Dincer, P. Berg, Journal of Power Sources 185 (2008) 1107–1114.
[27] A. Musa, H.J. Steeman, M.D. Paepe, Journal of Fuel Cell Science and Technology 4 (2007) 65–71.
[28] X. Li, Principles of Fuel Cells, Taylor & Francis, New York, 2005.
[29] A. Boden, G. Lindbergh, Journal of the Electrochemical Society 153 (2006) A2111–A2119.
[30] H. Wu, X. Li, P. Berg, International Journal of Hydrogen Energy 32 (2007) 2022–2031.
[31] I. Dincer, M.A. Rosen, Exergy, Energy, Environment and Sustainable Development, Elsevier, 2007.
[32] M.M. Hussain, J.J. Baschuk, X. Li, I. Dincer, International Journal of Thermal Sciences 44 (2005) 903–911.
[33] W.M. Haynes (Ed.), CRC Handbook of Chemistry and Physics, 91st edition, CRC Press/Taylor and Francis, 2011, internet version.
[34] S.H. Chan, C.F. Low, O.L. Ding, Journal of Power Sources 103 (2002) 188–200.
[35] J.H. Koh, H.K. Seo, Y.S. Yoo, H.C. Lim, Chemical Engineering Journal 87 (2002) 367–379.